A&A 440, 477–485 (2005)
DOI: 10.1051/0004-6361:20041642

Astronomy & Astrophysics

Radio, millimeter and optical monitoring of GRB 030329 afterglow: constraining the double jet model⋆

L. Resmi[1,2], C. H. Ishwara-Chandra[3], A. J. Castro-Tirado[4], D. Bhattacharya[1], A. P. Rao[3], M. Bremer[5], S. B. Pandey[6], D. K. Sahu[7,8], B. C. Bhatt[7], R. Sagar[6], G. C. Anupama[7], A. Subramaniam[7], A. Lundgren[9,10], J. Gorosabel[4], S. Guziy[4,11], A. de Ugarte Postigo[4], J. M. Castro Cerón[12], and T. Wiklind[12]

[1] Raman Research Institute, Bangalore 560080, India
e-mail: resmi@rri.res.in
[2] Joint Astronomy Programme, Indian Institute of Science, Bangalore 560012, India
[3] National Center for Radio Astrophysics, Post Bag 3, Ganeshkhind, Pune 411007, India
[4] Instituto de Astrofísica de Andalucía, Apartado de Correos, 3.004, 18080 Granada, Spain
[5] IRAM – Institut de Radio Astronomie Millimétrique, 300 rue de la Piscine, 38406 Saint-Martin d'Hères, France
[6] Aryabhatta Research Institute of Observational Sciences, Manora Peak, Naini Tal 263129, India
[7] Indian Institute of Astrophysics, Bangalore 560034, India
[8] Center for Research & Education in Science & Technology, Hosakote, Bangalore 562114, India
[9] European Southern Observatory, Alonso de Córdova, Casilla 19001, Chile
[10] Stockholm Observatory, 106 91 Stockholm, Sweden
[11] Astronomical Observatory, Nikolaev State University, Nikolskaja, 24, Nikolaev 54030, Ukraine
[12] Space Telescope Science Institute, 3.700 San Martín Dr., Baltimore, MD 21.218-2.463, USA

Received 12 July 2004 / Accepted 12 April 2005

Abstract. We present radio, millimeter and optical observations of the afterglow of GRB 030329. $UBVR_CI_C$ photometry is presented for a period of 3 h to 34 days after the burst. Radio monitoring at 1280 MHz has been carried out using the GMRT for more than a year. Simultaneous millimeter observations at 90 GHz and 230 GHz have been obtained from the Swedish-ESO Submillimeter Telescope (SEST) and the IRAM-PdB interferometer over more than a month following the burst. We use these data to constrain the double jet model proposed by Berger et al. (2003) for this afterglow. We also examine whether instead of the two jets being simultaneously present, the wider jet could result from the initially narrow jet, due to a fresh supply of energy from the central engine after the "jet break".

Key words. gamma rays: bursts

1. Introduction

The Gamma Ray Burst of 29th March 2003 has been an unique event. At a distance of ~870 Mpc (assuming a cosmology of $\Omega_\Lambda = 0.7$ and $\Omega_m = 0.3$, and a redshift of 0.1685 (Greiner et al. 2003a) it is the second nearest GRB for which an afterglow has been observed. The optical and radio afterglow of this burst has been one of the brightest detected till date (Peterson & Price 2003). The spectral signature of a supernova (SN2003dh) emerged in the optical transient a few days after the burst (Stanek et al. 2003) and thus provided the first unambiguous evidence of the long suspected association between Gamma Ray Bursts and Supernovae. Multifrequency observations indicated that the GRB consisted of at least two jet-like components of ejection with different opening angles and Lorentz factors, in addition to the supernova component (Berger et al. 2003).

GRB 030329 was detected and localized by the HETE-II satellite (Vanderspek et al. 2003a). The trigger H2652 occurred on 29th March 2003, at UT 11:37:14.7 and lasted more than 100 s. This was one of the brightest bursts detected by the instrument, with a 30–400 KeV fluence of 1.1×10^{-4} erg cm^{-2}. The Soft X-ray Camera on board HETE – II localized the burst to be at RA (J2000) = $10^h44^m49^s$ and Dec (J2000) = $+21°28'44''$ within an error circle of radius 2 arcmin. The temporal profile showed two distinct peaks in the burst, separated by ~11 s. Fluence in the lower energy band, $S_{(7-30\ \mathrm{KeV})}$, was 5.5×10^{-5} erg cm^{-2}, which implies a hardness ratio of $S_{(7-30\ \mathrm{KeV})}/S_{(30-400\ \mathrm{KeV})} > 0.33$, classifying this GRB into the "X-ray rich" category (Vanderspek et al. 2004). In a worldwide observational campaign, the afterglow was detected in all possible wavebands. The first X-ray detection by *RXTE* ~ 5 h after the burst found the source to be extremely bright with

⋆ Table 2 is only available in electronic form at http://www.edpsciences.org

a 2−10 KeV flux of 1.4×10^{-10} erg cm^{-2} s^{-1} (Marshall & Swank 2003). The optical transient had an R-band magnitude ∼12 when it was reported by Peterson & Price (2003) and Torii (2003). The VLA detected a bright 3.5 mJy radio afterglow at 8.46 GHz (Berger et al. 2003) on 2003 March 30.06 UT. Later follow up observations in other radio frequencies were reported by Pooley et al. (2003), Rao et al. (2003a,b), Hoge et al. (2003) and Kuno et al. (2003). Around 7 days after the burst the optical spectrum showed the signature of an underlying supernova emission (Stanek et al. 2003; Hjorth et al. 2003; Matheson et al. 2003), and the presence of the associated supernova SN2003dh was confirmed later by spectroscopic measurements. Continued monitoring has provided an unprecedentedly rich temporal coverage of the transient in all wavebands (Lipkin et al. 2004; Tiengo et al. 2003; Sheth et al. 2003; Berger et al. 2003; Guziy et al. 2005; Gorosabel et al. 2005a).

We present in this paper the observations done by an Indo-European GRB collaboration at radio, millimeter and optical wavelengths over a total observing span of nearly one year. The millimeter observations were conducted for more than a month at ESO and IRAM. Radio observations at a frequency of 1280 MHz were carried out with the Giant Meter Wave Radio Telescope (GMRT) (`http://www.ncra.tifr.res.in`) operated by the National Center for Radio Astrophysics, Pune. Optical follow-up was conducted till 34 days after the burst using the 2.01 m Himalayan Chandra Telescope (HCT) of the Indian Astronomical Observatory (IAO), Hanle and the 1.04 m Sampurnanand Telescope (ST) at the State Observatory, Naini Tal, now renamed as Aryabhatta Research Institute of Observational Sciences (ARIES). The GMRT observations represent the lowest frequency detection and the longest follow-up of the afterglow reported so far. This is also the first detection of a GRB afterglow by the GMRT. Our optical observations in $UBVR_{\rm C}I_{\rm C}$ pass-bands started ∼3 h after the burst. Except in the R band, these represent the earliest photometry of the optical transient. Our optical data also fill many temporal gaps existing in the literature (e.g. Lipkin et al. 2004). At millimeter waves, we used the SEST to make an early detection (∼0.6 days) at 86 GHz, albeit at low statistical significance, and subsequently monitored the burst until June 19, 2003, using the IRAM Plateau de Bure interferometer, making several simultaneous detections at frequencies ranging from 86 to 240 GHz. The early evolution of the optical afterglow followed the familiar behavior of a power-law decay in the light curve, with a steepening ("jet break") around 0.5 days (Garnavich et al. 2003; Smith 2003; Price et al. 2003). The nature of the optical light curve, however, deviated from this simple model after ∼1.5 days, displaying substantial variability and some change in average slope (see Lipkin et al. 2004 for a full compilation). At radio frequencies, the evolution of the afterglow flux was much slower than the early optical decay, and a steepening of the light curve was observed at ∼10 days after the burst (Berger et al. 2003). In order to explain this behavior, Berger et al. (2003) introduced a double-jet model, with a narrow jet responsible for the early optical emission and a wider jet contributing to the radio and late-time optical and X-ray emission. In addition, the optical light curve also has a significant contribution from the underlying supernova SN2003dh after about a week following the burst. The sharp bump in the optical light curve seen at ∼1.5 days has been attributed by Berger et al. (2003) to the deceleration epoch of the wider jet.

Granot et al. (2003) have instead proposed that the bump in the R-band lightcurve at 1.5 days and at three successive epochs could be attributed to refreshed shocks (see also Guziy et al. 2005). In their original model, however, the second jet break at ∼10 days was not expected (Piran et al. 2003).

In this paper, we examine the ability of the double jet model of Berger et al. to fit our observations along with other multi-band observations reported in the literature. We present a refined set of parameters for the two jets resulting from our fits. We also examine whether the two jets are in fact distinct entities or whether a refreshed shock might have converted the decelerating narrow jet to a wider, more energetic jet. In Sects. 2, 3 and 4 we describe respectively our radio, millimeter and optical observations, in Sect. 5 we present theoretical model fits and in Sect. 6 we discuss their implications. In Sect. 7 we calculate the reverse shock emission expected from the model. In Sect. 8 we estimate the possible contribution from SN2003dh. Section 9 summarizes our results.

2. Radio observations

We obtained radio observations at the center frequency of 1280 MHz using the Giant Meter Wave Radio Telescope (GMRT) located at Khodad, near Pune in Western India. GMRT is operated by the National Center for Radio Astrophysics. The telescope is an interferometric array of 30 fully steerable parabolic dishes of 45 m diameter each, spread over a distance of up to 25 km. The telescope operates at several spot frequencies between 150 to 1500 MHz, with a maximum bandwidth of 32 MHz at any given band. All feeds provide dual polarization outputs. The highest angular resolution achievable ranges from about 20 arcsec at the lowest frequencies to about 2 arcsec at 1.5 GHz. More details about the GMRT can be found in Swarup et al. (1991).

We made the first detection of the GRB 030329 radio transient in 1280 MHz band on 31st March 2003, 2.3 days after the GRB trigger (Rao et al. 2003a). The source was bright, with a flux of 0.33 mJy, 8σ above the background rms noise. Since then we have carried out a series of monitoring observations at the center frequency of 1280 MHz, at nine epochs until April 18, 2004. We used a bandwidth of 32 MHz during these observations. The flux scale is set by observing the primary calibrator 3C 286, 3C 147 or 3C 48. A phase calibrator was observed before and after a 30 to 45 min scan on GRB 030329. The integration time was 16 s. The data recorded from GMRT have been converted to FITS and analyzed using Astronomical Image Processing System (`AIPS`). At each epoch, the stability of the flux scale was checked by measuring the fluxes of a few background sources. The flux of background sources were consistently stable at all epochs, and the rms fluctuation in their flux (estimated to be 8%) has been taken as the error in the flux calibration. The final error quoted is the quadrature sum of the measurement error and the flux calibration uncertainty. The rms

Table 1. 1280 MHz radio observations at GMRT.

	Mid UT	Flux (mJy)
2003		
	Mar. 31 18:30	0.33 ± 0.09
	Apr. 1 20:30	0.33 ± 0.09
	May 30 16:30	1.10 ± 0.15
	Jun. 28 11:00	1.40 ± 0.16
	Aug. 9 07:30	2.50 ± 0.25
	Oct. 20 05:00	1.50 ± 0.17
	Dec. 3 00:20	1.30 ± 0.14
2004		
	Jan. 29 22:12	1.20 ± 0.18
	Apr. 18 14:32	1.10 ± 0.12

noise in the image is estimated from a sufficiently large area where no source was visible. The rms noise ranged from 35 to 80 μJy on different epochs. The radio transient was detected in all our observations. The flux showed an initial rise, reaching a peak of 2.5 mJy at ∼133 days after the burst followed by a secular decay (Table 1). As mentioned in Sect. 5, the observed nature of the 1280-MHz light curve tightly constrains the non-relativistic transition of the expanding jet.

3. The millimeter face of the afterglow

The first, single dish, observations were carried out on March 29−30, 2003 at La Silla, Chile, with the 15 m Swedish-ESO Submillimeter Telescope (SEST, Booth et al. 1989). We used the dual channel IRAM SIS-receiver, which allows simultaneous observations at 1.3 and 3 mm wavelengths. The 1.3 mm receiver was tuned to 215.0 GHz and the 3 mm receiver was tuned to 86.243 GHz. The backend used was a 3-level correlator with 2000 channels and the bandwidth was 1028 MHz for the 215 GHz receiver, and 512 MHz for the 86 GHz receiver. We used a dual beam switch mode (12 arcmin throw in azimuth) and integrated for 60 s (on source) per measurement. Observations were performed over three nights (see Table 3). During the observations the sky was clear and stable. The pointing was checked before and after the observations each night and was found to be stable within ±3″.

The intensity scale was calibrated using the standard chopper wheel method, with an internal calibration error of ∼10−20%. The intensity scale is converted from K to Jy using 40 Jy/K and 25 Jy/K for the 86 GHz and 215 GHz measurements respectively. Two blank sky integrations were done in order to test the performance of the receiver system (see Table 3). These observations were done during day time, resulting in higher noise levels (16 ± 164 and 4 ± 492 mJy respectively) than the observations of GRB 030329 which were done at night time. The blank sky observations did not produce reliable results at 215 GHz.

In order to derive the continuum level, each individual scan was inspected for spikes (which were removed) and abnormal baseline curvature. The average continuum and an estimate of the noise rms were derived for the central 400 MHz of the 86 GHz spectra, and 700 MHz of the 215 GHz spectra. The subscans were subsequently added together, weighted with their individual noise rms. Scans deviating by more than 3 sigma from this initial analysis were removed and the procedure repeated with the remaining scans. This generally does not change the average continuum flux, but decreases the dispersion. The final average continuum fluxes are given in Table 4. The dispersion in the continuum fluxes among individual scans are given as the 1σ error in Table 4.

Table 3. Results of the ESO/SEST scans on GRB 030329.

UT date of 2003	Freq. (GHz)	flux (mJy)	Beam
Mar. 29/30	86	82 ± 52	57″
	215	201 ± 308	23″
Mar. 30/31	86	−2 ± 78	57″
	215	−49 ± 262	23″
Mar. 31/Apr. 1	86	38 ± 65	57″
	215	−144 ± 250	23″

The dispersion in the measured continuum level, using the present technique, reflects the variable sky background and the inherent calibration uncertainty. It does not follow a normal distribution and increasing the number of subscans does not necessarily decrease the dispersion. The dispersion of continuum fluxes follows more a top-hat distribution. As such, it is not a good measure of the precision of the final continuum flux value, but nevertheless the only measure of the uncertainty at our disposal.

Under clear and stable weather conditions, as was the case for the SEST observations of GRB 030329, the average flux value is usually a robust estimate if the number of subscans is sufficiently large (e.g. >20). The flux value derived for the night of March 29 is higher than any of the following measurements, while the noise rms remains more or less constant. This is a strong indication that continuum flux was detected during the first night but not during the following nights. The weather conditions at the higher frequency band (215 GHz) were worse than at 86 GHz. We therefore conclude that at least at 3 mm (86 GHz), we did tentatively detect continuum flux during March 29, at a level around 80 mJy. The uncertainty associated with this, however, remains poorly defined and the quoted flux value should be regarded as approximate. At a 2σ level, the quoted uncertainty gives an upper bound of ∼104 mJy on the flux of the source.

At Plateau de Bure interferometer (Guilloteau et al. 1992), we carried out simultaneous observations in two bands, around 90 GHz and 230 GHz, the actual band center frequencies being slightly different on different days. The instrument was operating on compact D configuration with six antennas (6Dp) until May 3rd and with fewer antennas later (see Table 4). Data reduction and analysis was performed with the GLIDAS (Grenoble Image and Line Data Analysis) software. The target was observed at coordinates RA (2000) = $10^{\rm h}44^{\rm m}50.030^{\rm s}$, Dec (2000) = +21°31′18.15″ and the best position offsets were found on 31 Mar. 2003 to be: −0.87″ ± 0.03″ and −0.78″ ± 0.02″ respectively. Therefore, the absolute

Table 4. Results of the IRAM/PdB scans on GRB 030329.

UT date of 2003	Config.	freq (GHz)	flux (mJy)	Beam and PA
31 Mar. 00:04 to 03:07	6Dp	86.253	58.6 ± 0.5	14.1″ × 4.0″ at 55°
		232.032	46.8 ± 3.1	5.2″ × 1.5″ at 55°
31 Mar. 18:33 to 23:57	6Dp	98.473	58.2 ± 0.6	6.4″ × 4.2″ at 98°
		238.500	40.6 ± 2.1	2.8″ × 1.6″ at 84°
1 Apr. 20:20 to 21:55	6Dp	86.673	51.7 ± 0.9	9.1″ × 4.2″ at 98°
		240.528	23.8 ± 3.2	3.9″ × 1.6″ at 100°
5 Apr. 16:54 to 18:04	6Dp	115.447	40.4 ± 3.7	10.3″ × 3.1″ at −53°
10 Apr. 17:42 to 19:12	6Dp	86.244	23.5 ± 0.4	11.0″ × 4.2″ at −62°
		232.171	12.8 ± 1.3	4.5″ × 1.5″ at −65°
14 Apr. 20:10 to 22:16	6Dp	91.333	14.9 ± 0.4	8.1″ × 4.2″ at 84°
		217.029	9.2 ± 2.2	3.6″ × 1.7″ at 80°
18 Apr. 19:39 to 21:10	6Dp	115.271	7.7 ± 1.0	6.3″ × 3.3″ at 90°
		232.032	6.5 ± 1.8	3.3″ × 1.5″ at 87°
24 Apr. 17:36 to 19:32	6Dp	96.250	4.7 ± 0.7	8.2″ × 4.0″ at −67°
		241.480	0.0 ± 3.8	3.5″ × 1.4″ at 105°
3 May 15:59 to 19:49	6Dp	86.243	2.9 ± 0.3	9.5″ × 4.4″ at 108°
		233.467	1.4 ± 1.3	3.6″ × 1.6″ at −76°
16 May 13:20 to 15:57	5Dp	86.243	1.1 ± 0.8	12.4″ × 5.3″ at −54°
		231.490	0.0 ± 10.1	4.6″ × 1.9″ at −59°
28 May 21:29 to 23:22	5Dp	84.443	0.4 ± 0.7	16.6″ × 5.5″ at 52°
		238.500	0.0 ± 8.0	5.5″ × 1.9″ at 52°
20 June 12:41 to 17:49	4Dp	95.434	0.6 ± 1.3	5.92″ × 5.63″ at 64°

coordinates are RA (2000) = $10^{h}44^{m}49.968^{s}$(±0.002 s), Dec (2000) = +21°31′ 17.″37(±0.02″). Thus, within the error limits, the measured position definitely stays constant throughout the observing period. The source has been detected up to May 3rd, after which there are only upper limits available.

4. Optical observations and data reduction

Starting about 3 h after the burst, we obtained a total of 13, 70, 87, 167, and 39 photometric observations in Johnson *U*, *B*, *V* and Cousins *R* and *I* bands respectively, from both ST and HCT. The CCD used at HCT was 1024×1024 pixel^2 with the entire chip covering a field of ∼4.′7 × 4.′7 on the sky. It has a read out noise of 11 e^- and gain of 4.8 e^-/ADU. A CCD chip of size 2048×2048 pixel^2 was used at ST, which covers a field of ∼13′ × 13′. The gain and read out noise are 10 e^-/ADU and 5.3 e^- respectively. The frames were binned in 2×2 pixel^2 to improve the signal-to-noise ratio of the source. Several twilight flat field and bias frames were obtained for the CCD images at both the telescopes. While imaging the optical transient (OT), several short exposures upto a maximum of 15 min were taken in various filters. We used MIDAS, IRAF and DAOPHOT softwares to process the CCD frames in the standard fashion. The bias subtracted and flat fielded CCD frames were co-added, whenever found necessary.

The *BVRI* magnitudes of the OT obtained from the Sampurnanand Telescope at Naini Tal were calibrated differentially using secondary standard stars Nos. 1, 11, 14, 19, 37 and 57 in the list of Henden (2003), while the *U* magnitudes were determined using reference stars 1, 11 and 37 from Henden (2003). *BVR* magnitudes obtained at the IAO were also calibrated differentially, using reference stars Nos. 14, 18 and 19 of Henden (2003). OT magnitudes at similar epochs, determined using photometry from the two sites, are consistent with each other within the limits of uncertainty. A full compilation of our data is presented in Table 2.

Figure 1a displays our *UBVRI* photometry (open circles) along with some of the data published by other authors (filled circles). As mentioned above, in *UBVI* bands we report the earliest observations and in all the bands our observations fill in gaps in photometric data reported in the literature so far, at epochs beyond one day after the burst.

Reported X-ray observations of this afterglow are shown in an accompanying Fig. 1b. The role of the X-ray observations in constraining the model, along with observations in other bands, is discussed in Sect. 5.

5. Modeling the multiband observations

It was proposed by Rhoads (1999) that the explosion which makes the GRB may not be isotropic. Ejection of matter in the explosion could in fact be collimated within narrow cones. If so, then a signature of this collimation is expected in the form of an achromatic steepening ("jet break") in the afterglow light

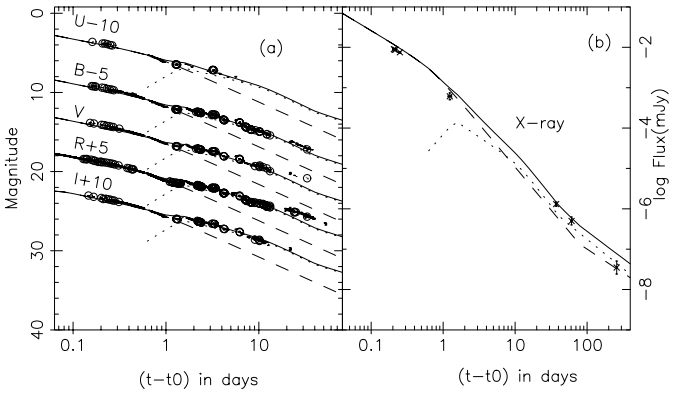

Fig. 1. a) The optical lightcurve of the afterglow of GRB 030329. Open circles represent the data presented in this paper and filled circles are those from the literature (Lipkin et al. 2004). The solid line shows the total flux predicted by model 1 discussed in the text, which has two jets as in Berger et al. (2003). The dashed line shows the contribution of the narrow jet alone and the dotted line that of the wide jet in each band. **b)** X-ray observations reported by Tiengo et al. (2003, 2004), shown along with the prediction of model 1. Contribution of the narrow jet and the wide jet are shown separately as the dashed and the dotted line respectively. The total flux is shown as the solid curve.

curve (Rhoads 1999; Sari et al. 1999). The jet break appears when the Lorentz factor of the expanding outflow drops below the inverse of the initial angle of collimation, causing the lateral expansion of the jet to dominate over its radial motion. This behavior has now been observed in a number of afterglows (see reviews by Piran 2004 and Sagar 2002).

5.1. The double jet model for GRB 030329

The X-ray and optical lightcurves of GRB 030329 afterglow had an initial temporal slope of ~ -0.9. Around half a day, the optical decay steepened to an index of ~ -1.9. Sampling of the X-ray evolution was poor, but an interpolation of the *RXTE* and *XMM* data obtained during ~0.1 to ~100 days indicated a break almost at the same time as the optical steepening mentioned above (Tiengo et al. 2003). A nearly simultaneous break observed in frequencies separated by four orders of magnitude suggested that the break observed at ~0.5 days was a jet break.

At radio frequencies, the first observations obtained were around 1 days, somewhat later than the epoch of the jet break obtained from optical and X-ray observations. The radio and millimeter light curves, however, did not display the behavior expected after a jet break at 0.5 days. Instead, they were rather well described by a second jet, with a jet break around 10 days (Berger et al. 2003; Sheth et al. 2003). The optical light curve showed a re-brightening around 1.5 days, followed by a slower decay consistent with that expected from the second jet to which the radio emission was attributed (Berger et al. 2003; Lipkin et al. 2004). This led Berger et al. (2003) to propose a double-jet model for GRB 030329. The optical re-brightening at 1.5 days was attributed to the epoch of deceleration of the second jet. Berger et al. (2003) estimated the initial opening angle of the first (narrow) jet to be ~5° and that of the second (wide) jet to be ~18.4°. The energy contents of the two jets were estimated to be $\sim 6.7 \times 10^{48}$ erg for the narrow jet and $\sim 10^{49}$ erg for the wide jet. Compared to the narrow jet, a later deceleration epoch implied a smaller initial Lorentz factor for the wide jet, and correspondingly a much higher initial baryon load. The double jet model has been found to be consistent with most observations reported till date. The optical emission at late times ($t > 10$ days) is, however, dominated by the associated supernova SN2003dh.

We attempted modeling our observations along with multiwavelength data available in the literature within the ambit of this double-jet model (model 1). The basic quantity in our model is the synchrotron source function, which we consider to have appropriate power-law forms between the usual break frequencies. Transition from one power-law phase to another is made gradual through a Band type smoothening (Band et al. 1993) at the peak frequency ν_m and the cooling frequency ν_c. The self-absorption frequency ν_a is not treated as a break; instead the absorption is incorporated into the expression for synchrotron optical depth, which, along with the source function, yields the flux at any given frequency. In the co-moving frame of the shock, the optical depth is set to unity at $\nu = \nu_a$ (co-moving). We incorporate transition to a non-relativistic phase of expansion, as in Frail et al. (2000). The non-relativistic transition is treated as a sharp break at a time $t = t_{nr}$. We obtain our fits through the usual χ^2 minimization procedure, using $\nu_a, \nu_m, \nu_c, t_{nr}$, the electron distribution index p and the jet break time t_j as the fit parameters. Here we are trying to model the underlying smooth power law behavior rather than the short time scale variabilities in the lightcurve. Since our model does not include the short-term variabilities, the nominal χ^2 obtained is relatively high. The best fit from this model is shown in Figs. 1 and 2. We derived the physical parameters E_{iso} (the isotropic equivalent energy of the burst), n (number density of the ambient medium), ϵ_e and ϵ_B (fractional energy content in the electrons and in the magnetic field respectively) using the expressions in Wijers & Galama (1999) from these fitted parameters, with appropriate modifications to place ν_a at $\tau_\nu = 1$ instead of 0.35 used by Wijers & Galama (1999).

5.1.1. The wide jet

The parameters of the wide jet are well constrained by data in the 4–250 GHz range, as discussed by Berger et al. (2003) and Sheth et al. (2003). At the jet break time of 9.8 days, we find the self absorption frequency ν_a to be $1.3^{+0.25}_{-0.06} \times 10^{10}$ Hz, the synchrotron peak frequency ν_m to be $3.98^{+0.5}_{-0.1} \times 10^{10}$ Hz with a peak flux F_m of $44.7^{+1.0}_{-2.0}$ mJy. The post jet-break decay in radio, the peak optical flux at 1.5 days and the late X-ray observations at 37 and 61 days together constrain the electron energy distribution index p to $2.3^{+0.05}_{-0.02}$ and the cooling frequency ν_c to $3.98^{+1.3}_{-2.0} \times 10^{14}$ Hz after the jet break. These parameter values are very similar to those derived by Berger et al. (2003). Our 1280 MHz observations show a gradual rise of flux to a peak around 133 days. This behavior can be reproduced by a non-relativistic transition of the jet at $t_{nr} = 42^{+17}_{-7}$ days.

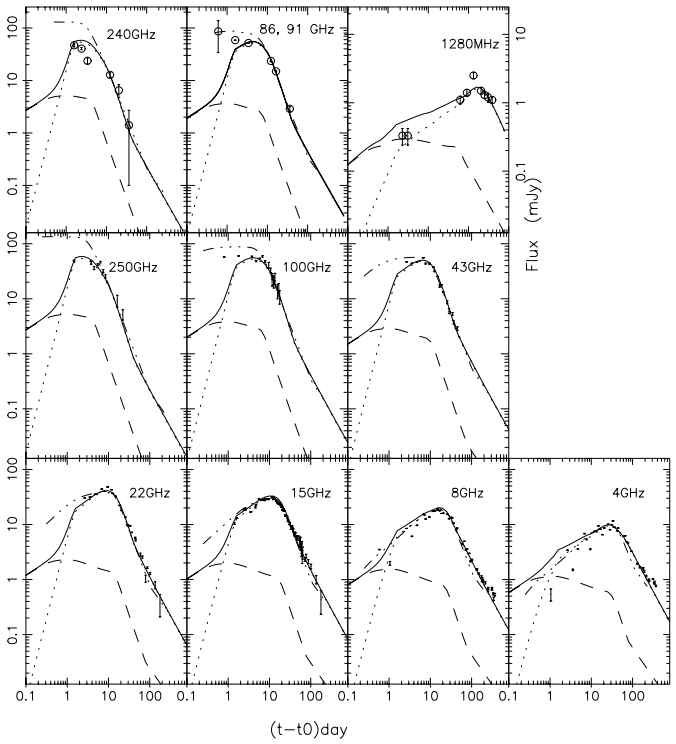

Fig. 2. Millimeter and radio observations of GRB 030329 afterglow along with the predictions of model 1 (two jets). Observations reported in this paper are represented by open circles, crosses are data points from Berger et al. (2003) and Sheth et al. (2003). The dashed and the dotted lines represent contributions of the narrow and the wide jet respectively, the solid line shows the sum. The dash-dot-dot line shows a model fit for an assumed stellar-wind density profile for the ambient medium.

5.1.2. The narrow jet

The jet break time for the narrow jet is derived to be $0.69^{+0.08}_{-0.06}$ days from the optical light curve. Using a galactic extinction $E(B-V) = 0.025$ mag in the direction of the GRB (Schlegel et al. 1998), the early optical and X-ray observations, both before and after this break, are well described by an electron energy distribution index p of 2.12 ± 0.05. Some authors (e.g. Sato et al. 2003; Lipkin et al. 2004) have conjectured that there occurs a passage of the cooling break (ν_c) through optical bands within the first few hours after the GRB, based on a derived change in slope of R-band light curve around ∼0.25 days, and a small color evolution. Our own observations have a continuous coverage from ∼0.15 days to ∼0.3 days after the burst, taken from the same instrument and calibrated uniformly on the same scale. We find that our data over this interval are fit very well by a single power law. Even the data reported by Lipkin et al. (2004) and Sato et al. (2003) do not conclusively demonstrate a secular steepening at ∼0.25 days; the effect could be easily mimicked by short-term variability riding on a single, underlying power law. Colors derived from our own multiband observations have somewhat large errors (∼0.08 mag 1-σ), and we are unable to discern the ∼0.1 mag systematic change in $B-R$ color reported by Lipkin et al. (2004). As mentioned by Lipkin et al. (2004), there could be various reasons for this early color evolution. We do not feel that the passage of cooling break through optical bands at early times can be conclusively established from the existing observations. From multiband fits, however, we estimate ν_c to be at $1.0^{+1.0}_{-0.5}\times10^{16}$ Hz at 0.5 days. At times >1.5 days, the contribution from the wide jet is sufficient to reproduce the radio light curves (see Fig. 2), so the radio emission from the narrow jet is constrained to be almost negligible. In order to achieve this, we need to have the peak frequency ν_m and the self absorption frequency ν_a of the narrow jet to be as high as possible. The passage of ν_m is not observed through the optical band, so we chose it to be just below the R-band at the earliest epoch (∼0.05 days) at which data are available. This results in ν_m regressing to $\sim10^{13}$ Hz at the jet break epoch of 0.5 days. The fitted peak flux $F_{(\nu=\nu_m)}$ is $19.8^{+9.3}_{-2.4}$ mJy at this time. The density of the ambient medium can be derived from the rather well-constrained parameters of the wide jet, and works out to be $n \sim 8$ atom/cc. This, along with the narrow jet parameters mentioned above, predicts the self absorption frequency of the narrow jet to be ν_a equal to $3.1^{+0.14}_{-0.63}\times10^9$ Hz at 0.5 days. We find that this value of ν_a yields adequate suppression of the narrow jet flux at low frequencies for the model to be consistent with our 1280 MHz data.

As mentioned earlier, the $\chi^2_{\rm d.o.f.}$ is somewhat high due to short-term variabilities in the observed light curve. From the fit we excluded the first seven days of data at 4.86 and 8.46 GHz, which appear to have been affected by scintillations. The first data point at 250 GHz (∼1.5 days) and at 100 GHz (0.8 days) were also removed from the fit. We did not consider five more data points in radio bands (of 2.6 days in 43 GHz, days 1 and 12 in 22 GHz and days 3.5 and 4.7 in 15 GHz) which produced high χ^2 values due to scatter. We exclude the optical data from discussion for epochs larger than ∼5 days because of the dominant contribution from SN2003dh. A $\chi^2_{\rm d.o.f.}$ of 23.3 is obtained for the best fit with this model. The optical (mostly V and B) bands dominate the contribution to χ^2 along with the lower radio frequencies (4 GHz, 8 GHz and 15 GHz). The number density of the ambient medium is inferred to be 8.6^{+12}_{-5}. We infer the fractional energy content in relativistic electrons and magnetic field to be $0.56^{+0.4}_{-0.5}$ and $4^{+1.9}_{-1.8}\times10^{-4}$ respectively for the narrow jet, and $9.0^{+3}_{-1}\times10^{-2}$ and $11.9^{+10}_{-7}\times10^{-4}$ for the wide jet. We derive $1.4^{+1.3}_{-0.8}\times10^{51}$ erg for the isotropic equivalent energy and $6.2^{+0.02}_{-0.03}$ degrees for the opening angle of narrow jet. This corresponds to a total energy content of $3.3^{+4.8}_{-2.4}\times10^{48}$ erg in the jet. For the wide jet, we derive an isotopic equivalent energy of $1.2^{+0.4}_{-0.2}\times10^{50}$ erg, opening angle of $23.3^{+0.07}_{-0.04}$ degrees and a total energy of $5.0^{+3.3}_{-2.1}\times10^{48}$ erg.

We calculated the rising flux from the wide jet at $t < 1.5$ days, assuming time evolution of the spectral parameters to be of the form $\nu_m \propto t^0$, $\nu_c \propto t^{-2}$, $f_{\nu_m} \propto t^3$ (Peng et al. 2004) and $\nu_a \propto t^1$ and normalizing them at 1.5 days.

We also explored the possibility of the ambient medium of the burst being generated by a stellar wind, with a density profile of $n(r) \propto r^{-2}$, but were unable to obtain consistent fits with the double-jet model. If the model is tuned to reproduce radio data in the 8−43 GHz frequency range, it leads to an overprediction of fluxes in millimeter bands and an underprediction at 1280 MHz (cf. Fig. 2).

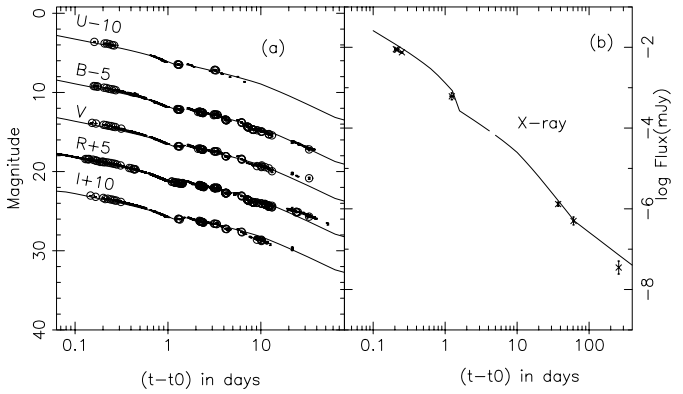

Fig. 3. a) The optical lightcurve of the afterglow of GRB 030329, shown with the prediction of model 2 (solid line), which assumes a transition of an initially narrow jet to a wider jet at ∼1.5 days. **b)** X-ray observations reported by Tiengo et al. (2003, 2004), with predictions of model 2. The flattening seen at late times is due to the transition into non-relativistic regime at ∼63 days.

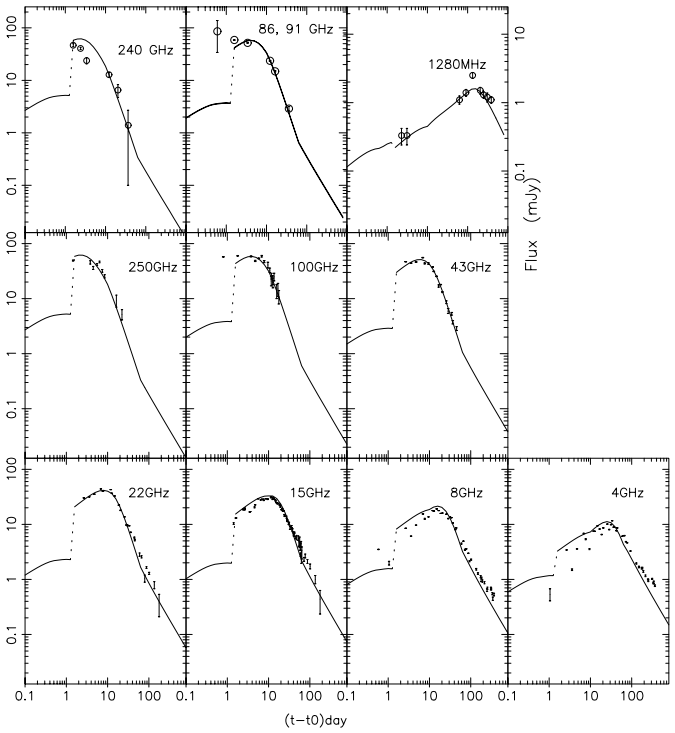

Fig. 4. Millimeter and radio observations of GRB 030329, along with the predictions of model 2 (refreshed jet) shown as the solid line. Open circles are data presented in this paper, crosses represent data taken from Berger et al. (2003) and Sheth et al. (2003).

5.2. Refreshed jet?

Most of the observations are well reproduced by a model which sums the contributions from the wide and narrow jet. We note that the contribution of the narrow jet is almost negligible at radio bands; in fact the wide jet alone is quite sufficient to account for the observed flux after ∼1.5 days. It therefore appears to us that the data could be well described if, instead of both jets contributing simultaneously to the emission, the narrow jet alone contributes at epochs earlier than ∼1.5 days, and only the wide jet after that time. This suggests that a possible re-energization event around or before ∼1.5 days could have refreshed the initially narrow jet, which had entered the lateral expansion phase, and given it additional forward momentum, converting it into the second, "wide" jet. The opening angle of the laterally expanding, initially narrow jet around ∼1.5 days is estimated to be ∼20°, not far from the initial opening angle inferred for the wide jet (∼23°). We therefore consider it possible that a re-energization event occurred after the jet break of the narrow jet as suggested by Granot et al. (2003) and the double-jet model for GRB 030329 could represent the conversion of an initially narrow jet to a wide one by the re-energization.

In a simple representation of such a re-energization, we assume that the physical parameters of the fireball, namely E, ϵ_e and ϵ_B undergo a change after re-energization, while the ambient density n remains the same. We allow these physical parameters to be determined by the model fits.

Fits to multiwavelength observations with this model (model 2) are shown in Figs. 3 and 4. We excluded the same set of data in these fits as done in model 1. The minimum $\chi^2_{\rm d.o.f.}$ we obtained with this model is 24.5, slightly higher than the value for the previous model. Here again, the χ^2 is dominated by the optical band as well as the low radio frequencies. Both model 1 and model 2 underpredict the flux at 1280 MHz peak by a factor of 2. But it is difficult to make a distinction between model 1 and model 2 from the small difference in the χ^2. Parameters for the initial, narrow jet are nearly the same as those listed in Sect. 5.1.2. except the self absorption frequency ν_a ($2.9^{+0.8}_{-0.06} \times 10^9$ Hz), which is implied by the value of n inferred from the parameters of the jet after re-energization. Parameters of the refreshed jet are only marginally different from that of the wide jet discussed in Sect. 5.1.1. We obtain a p of 2.24 ± 0.02, t_j of $10^{+2.3}_{-1.0}$ days, and at 9.8 days, a cooling frequency of $5.0^{+2.1}_{-1.5} \times 10^{14}$ Hz, and a marginally reduced self absorption frequency of $1.1^{+0.3}_{-0.05} \times 10^{10}$ Hz. The non-relativistic transition time t_{nr} is $63^{+13.5}_{-30}$ days. The number density of the ambient medium is inferred to be $6.7^{+13.}_{-3.}$. We infer the fractional energy content in relativistic electrons (ϵ_e) and magnetic field (ϵ_B) to be $0.53^{+0.5}_{-0.4}$ and $4^{+2.5}_{-1.3} \times 10^{-4}$ respectively for the initial (narrow) jet, and $0.103^{+0.05}_{-0.01}$ and $1.0^{+1}_{-0.5} \times 10^{-3}$ for the refreshed (wide) jet. We derive an isotropic equivalent energy of $1.2^{+1.6}_{-0.6} \times 10^{51}$ erg for the original jet, which has an initial opening angle of $5.9^{+0.3}_{-0.1}$ degrees. This corresponds to a total energy content of $3.2^{+6}_{-2.8} \times 10^{48}$ ergs in the jet. After re-energization, which is assumed to end around ∼1.5 days, the total energy content of the jet increases to $5.8^{+5.9}_{-1.7} \times 10^{48}$ erg, and the jet widens to $20.5^{+0.1}_{-0.03}$ degrees.

The transition to the refreshed physical parameters of the jet is expected to be gradual, over the time required to establish a new equilibrium. The timescale for achieving a new Blandford-McKee structure will be roughly equal to the time the second wave requires to cross the existing shocked shell. This time, in the co-moving frame, can be estimated as the thickness of the matter in the co-moving frame of the shock, divided by c, which in the observer's frame will be $\Delta t \approx R/(a\Gamma_{\rm old}\Gamma_{\rm new}c)$, where $a \sim 5{-}10$. At 1.5 days, when the new power law

phase begins, we calculate the bulk Lorentz factor ($\Gamma_{\rm new}$) to be ∼2.3, by extrapolating the value of Γ from the jet break time. Extrapolation for the initial jet produces $\Gamma_{\rm old}$ to be close to this value. Hence Δt will be of the order of 0.2–0.3 days. From a close examination of the optical lightcurve, we find that the refreshment episode could begin at ∼1.2 days and at ∼1.5 days, the new power law phase begins.

6. Discussion

We have seen above a comparison between the parameters of the two models. We now discuss their compatibility with the constraints imposed by other available observations of the afterglow. The angular size of the fireball estimated by Taylor et al. (2004) can be reproduced by models with isotropic equivalent energy to external density ratio in the range 10^{50}–10^{52} erg cm^{-3} (Oren et al. 2004). The parameters extracted from both the models fall close to this range.

Polarization measurements of the afterglow are available in optical (Greiner et al. 2003b) and in radio (Taylor et al. 2004) bands. In the optical, the degree of polarization decreases shortly after the jet break at ∼0.5 days and rapid variations in polarization start occurring around 1.5 days, which according to Greiner et al. could be the beginning of a new power law phase. The linear polarization at 8 GHz (<0.1%) around 8 days is significantly lower than the optical polarization (∼2%), which could be due to the fireball being optically thick at this frequency. This polarization behavior has been thought to support the double jet model (Greiner et al. 2003b; Taylor et al. 2004); however this is equally applicable to the refreshed jet.

We point out that the first millimeter-wave observation at 86 GHz by the SEST at 0.6 days and the 100 GHz observation reported by Sheth et al. (2003) at 0.8 days are not well fit by this simple model. Nor does the double-jet model of Berger et al. (2003) succeed in reproducing this well.

7. Reverse shock

It has been pointed out (Piran et al. 2003) that the deceleration of the wide jet at 1.5 days is expected to be accompanied by a strong radio flash from the reverse shock, which is not observed. This concern remains for the refreshed jet model, too. The two models differ in the nature of the medium in which the second shock front decelerates (in model 1, a normal ISM while in model 2, it is the material already shocked by the first shell). The Sedov length in these two cases are also to be evaluated differently, since in model 1, the shell responsible for the wide jet encounters matter all the way from the progenitor star while in model 2, the second wave of energy passes through the region evacuated by the first jet.

We estimated the reverse shock emission expected in either model, assuming that the shock is ultrarelativistic (thick shell case) (Sari & Piran 1995; Kobayashi 2000). For model 1 there are four relevant regions, namely, normal ISM (0), ISM shocked by the wide jet (1), reverse shocked ejecta (2) and the cold second shell (3). Region 1 and region 2 are separated by a contact discontinuity (CD). We followed the formulation of Kobayashi (2000) to obtain the flux expected from reverse shock. In model 2, since the reverse shock originates when the second wave of energy decelerates into the already shocked material, the space ahead of the CD will be divided into three regions instead of two (Kumar & Piran 2000). The five relevant regions in this case are: the ISM (0), the ISM shocked by the first wave (1), ISM additionally shocked by the second wave (2), reverse shocked ejecta (3) and the cold second shell (4). A contact discontinuity separates regions 2 and 3. Assuming pressure balance at the CD, and for the ejecta using the assumption that $n_4 R^2$ is constant, (where n_4 is the number density of the cold shell and R is the distance to the CD), one obtains the bulk Lorentz factor (γ_3) and thermodynamic quantities (density and pressure) of region 3. These quantities allow one to estimate the synchrotron emission from that region. The thickness (Δ) of the ejecta is an unknown parameter in both models. For a given Δ the peak flux produced by model 1 is two orders of magnitude lower than model 2 at the deceleration time of 1.5 days. The computed flux is inversely related to Δ, and the minimum value Δ can reach without overpredicting the flux observed at various bands is $\sim 10^{10}$ cm for model 1, and $\sim 10^{13}$ cm for model 2. More detailed investigations taking into account detailed hydrodynamics in non-spherical geometry as well as the density structure of a post-jet break fireball may be necessary to get a better estimate.

8. SN2003dh

The optical emission observed at times later than ∼7 days cannot be fully accounted for by the afterglow models discussed so far. We attribute the excess emission at these late epochs primarily to the associated supernova, SN2003dh. We subtract the afterglow flux predicted by the model and the flux due to the host galaxy (Gorosabel et al. 2005b) from the observed data to estimate the contribution from the supernova. Figure 5 displays the flux attributed to the supernova in the two models discussed above. The K-corrected light curve of SN1998bw (Galama et al. 1998) appropriate for the redshift of GRB 030329 is shown along with the residuals for comparison. While being similar in temporal behavior, the residuals from model 1 are fainter by ∼0.3 mag in comparison to an equivalent SN1998bw lightcurve. In case of model 2, this difference is ∼0.4 mag. These results compare well with the estimate of Lipkin et al. who find that an SN1998bw lightcurve, diminished by 0.3 mag, is required to fit the observed data.

9. Summary

We have presented low frequency radio, millimeter wave and optical observations of the afterglow of GRB 030329, and interpreted them in terms of the double-jet model discussed earlier in the literature. Our main conclusions are summarized below.

– The 1280 MHz GMRT observations, starting ∼2 days after the burst and continuing for over a year, provide constraints on the self absorption frequency of the emission region as well as the epoch of non-relativistic transition of the fireball.

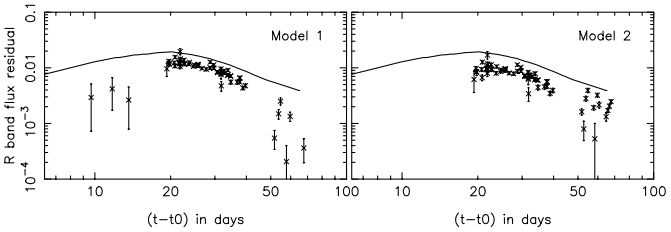

Fig. 5. *R*-band residuals for epochs beyond ∼7 days, after subtracting the modeled flux of the afterglow and the contribution of the host galaxy (R = 22.6, Gorosabel et al. 2005b) from the observed flux. The two models are shown in adjacent panels. This shows the *R*-band contribution needed from the associated supernova SN2003dh to explain the total observed light from the OT. The solid line is the red-shifted K-corrected SN1998bw *R*-band lightcurve, shown for comparison.

- We report several simultaneous two-band (∼90 and ∼250 GHz) detections of the afterglow for over a month after the burst.
- Our optical observations span a temporal range of 3 h to 34 days and fill in many gaps in the coverage reported so far in the literature. In *UBVI* bands our data represent the earliest photometry of the optical transient.
- We find that the data can be well fit by a model where the two jets are present either simultaneously or in exclusion of each other. We derive a non-relativistic transition time of ∼42 days for model 1 and ∼63 days for model 2. Although concerns with reverse shock emission remain in both models, we deem it possible that the optical re-brightening seen at the epoch of ∼1.3 days could be a re-energization of the jet, which resulted in the initially narrow jet being converted into a more energetic wider jet.

Acknowledgements. The GMRT is operated by the National Center For Radio Astrophysics of the Tata Institute of Fundamental Research. This work is based partly on observations carried out with the IRAM Plateau de Bure Interferometer. IRAM is supported by INSU/CNRS (France), MPG (Germany) and IGN (Spain). The SEST observations were conducted as part of the GRACE Collaboration Program for the multiwavelength follow up of Gamma-ray Bursts at ESO with ID 70.D-0523. We thank the ESO and IRAM Plateau de Bure staff and their operators for their great support in the observations. The HCT is operated by the Indian Institute of Astrophysics, Bangalore. This paper makes use of data obtained through the High Energy Astrophysics Science Archive Research Center Online Service, provided by the NASA/Goddard Space Flight Center. The GCN system, managed and operated by Scott Barthelmy, is gratefully acknowledged. This research is partially supported by the Spain's Ministerio de Educación y Ciencia through programs ESP2002-04124-C03-01 and AYA2004-01515 (including FEDER funds). LR acknowledges financial support from Council for Scientific and Industrial Research, India. The authors thank an anonymous referee for critical comments which helped improve the paper.

References

Band, D., Matteson, J., Ford, L., et al. 1993, ApJ, 413, 281
Berger, E., Kulkarni, S. R., Pooley, G., et al. 2003, Nature, 426, 154
Berger, E., Soderberg, A. M., & Frail, D. A. 2003, GCNC, 2014
Booth, R., Delgado, G., Hagstrom, M., et al. 1989, A&A, 216, 315
Frail, D. A., Waxman, E., & Kulkarni, S. R. 2000, ApJ, 191
Galama, T. J., Vreeswijk, P. M., van Paradijs, J., et al. 1998, Nature, 395, 670
Garnavich, P., Stanek, K. Z., & Berlind, P. 2003, GCNC, 2018
Granot, J., Nakar, E., & Piran, T. 2003, Nature, 426, 138 [arXiv:astro-ph/0304563]
Greiner, J., Peimbert, M., Estaban, C., et al. 2003a, GCNC, 2020
Greiner, J., Klose, S., Reinsch, K., et al. 2003b, Nature, 426, 157
Gorosabel, J., Castro-Tirado, A. J., Guziy, S., et al. 2005a, in preparation
Gorosabel, J., Ramírez-Pérez, M. D., Sollerman, J., et al. 2005b, A&A, submitted
Guilloteau, S., Delannoy, J., Downes, et al. 1992, A&A, 262, 624
Guziy, S., Castro-Tirado, A. J., Jóhannesson, G., et al. 2005, in preparation
Henden, A. 2003, GCNC, 2082
Hjorth, J., Sollerman, J., Møller, P., et al. 2003, Nature, 423, 847
Hoge, J. C., Meijerink, R., Tilanus, R. P. J., & Smith, I. A. 2003, GCNC, 2088
Kobayashi, S. 2000, ApJ, 545, 807
Kumar, P., & Piran, T. 2000, ApJ, 532, 286
Kuno, N., Sato, N., & Nakanishi, H. 2003, GCNC, 2089
Lipkin, Y. M., Ofek, E. O., Gal-Yam, A., et al. 2004, ApJ, 606, L381
Marshall, F. E., & Swank, J. H. 2003, GCNC, 1996
Matheson, T., Garnavich, P. M., Foltz, C., et al. 2003, ApJ, 582, L5
Oren, Y., Nakar, E., & Piran, T. 2004 [arXiv:astro-ph/0406277]
Peng, F., Königl, A., & Granot, J. 2004, ApJ, submitted [arXiv:astro-ph/0410384]
Peterson, B. A., & Price, P. A. 2003, GCNC, 1985
Piran, T. 2005, Rev. Mod. Phys., 76, 1143
Piran, T., Nakar, E., & Granot, J. 2003 [arXiv:astro-ph/0312138], Talk given by T. Piran at the GRB Symposium, Santa Fe, September, 2003
Pooley, G. 2003, GCNC, 2043
Price, P. A., Fox, D. W., Kulkarni, S. R., et al. 2003, Nature, 423, 844
Rao, A. P., Ishwara-Chandra, C. H., & Bhattacharya, D. 2003a, GCNC, 2073
Rao, A. P., Ishwara-Chandra, C. H., Bhattacharya, D., & Castro-Tirado, A. J. 2003b, GCNC, 2268
Rhoads, J. E. 1999, ApJ, 525, 737
Sagar, R. 2002, BASI, 30, 237
Sari, R., & Mészáros, P. 2000, ApJ, 535, L33
Sari, R., & Piran, T. 1995, ApJ, 455, L143
Sari, R., Piran, T., & Halpern, J. P. 1999, ApJ, 590, L17
Sato, R., Kawai, N., Suzuki, M., et al. 2003, ApJ, 599, L9
Schlegel, D. J., Finkbeiner, D. P., & Davis, M. 1998, ApJ, 500, 525
Sheth, K., Frail, D. A., White, S., et al. 2003, ApJ, 595, L33
Smith, D. A. 2003, GCNC, 2019
Stanek, K. Z., Matheson, T., Garnavich, P. M., & Martini, P. 2003, ApJ, 591, L17
Swarup, G., Ananthakrishnan, S., Kapahi, V. K., et al. 1991, Curr. Sci., 60, 95
Taylor, G. B., Frail, D. A., Berger, E., & Kulkarni, S. R. 2004, ApJ, 609, L1
Tiengo, A., Mereghetti, S., Ghisellini, G., et al. 2003, A&A, 409, 983
Tiengo, A., Mereghetti, S., Ghisellini, G., Tavecchio, F., & Ghirlanda, G. 2004, A&A, 423, 861
Torii, K. 2003, GCNC, 1986
Vanderspek, R., Crew, G., Doty, J., et al. 2003a, GCNC, 1997
Vanderspek, R., Sakamoto, T., Barraud, C., et al. 2004, ApJ, 617, 1251
Wijers, R. A. M. J., & Galama, T. J. 1999, ApJ, 523, 177

Online Material

Table 2. Optical transient.

	Date (UT)	Time since Burst in days	Magnitude (mag)	Exposure time (s)	Telescope
		$U-$passband			
2003	March				
	29.6459	0.1619	13.606 ± 0.051	200	ST
	29.6918	0.2078	13.824 ± 0.052	200	ST
	29.7042	0.2202	13.831 ± 0.060	200	ST
	29.7186	0.2346	13.910 ± 0.061	200	ST
	29.7345	0.2505	14.016 ± 0.053	200	ST
	29.7477	0.2637	14.069 ± 0.051	200	ST
	30.7558	1.2718	16.454 ± 0.053	300	ST
	30.7738	1.2898	16.486 ± 0.057	300	ST
	30.7909	1.3069	16.483 ± 0.056	300	ST
	30.8084	1.3244	16.507 ± 0.063	300	ST
2003	April				
	1.6524	3.1684	17.156 ± 0.061	400	ST
	1.7046	3.2206	17.153 ± 0.058	400	ST
	1.7626	3.2786	17.201 ± 0.055	400	ST
		$B-$passband			
2003	March				
	29.6429	0.1589	14.189 ± 0.026	150	ST
	29.6483	0.1643	14.1463 ± 0.070	900	HCT
	29.6552	0.1712	14.248 ± 0.032	100	ST
	29.6603	0.1763	14.1933 ± 0.046	900	HCT
	29.6891	0.2051	14.409 ± 0.031	100	ST
	29.7013	0.2173	14.440 ± 0.022	100	ST
	29.7153	0.2313	14.534 ± 0.012	200	ST
	29.7312	0.2472	14.599 ± 0.016	200	ST
	29.7445	0.2605	14.653 ± 0.014	200	ST
	29.7574	0.2734	14.704 ± 0.028	200	ST
	30.7378	1.2538	17.0433 ± 0.033	900	HCT
	30.7598	1.2758	17.137 ± 0.015	200	ST
	30.7730	1.289	17.0573 ± 0.060	900	HCT
	30.7776	1.2936	17.170 ± 0.016	200	ST
	30.7948	1.3108	17.167 ± 0.014	200	ST
	30.8123	1.3283	17.192 ± 0.016	200	ST
	30.8359	1.3519	17.0923 ± 0.032	900	HCT
	31.5978	2.1138	17.464 ± 0.032	300	ST
	31.6707	2.1867	17.3683 ± 0.053	900	HCT
	31.6763	2.1923	17.421 ± 0.032	300	ST
	31.6984	2.2144	17.472 ± 0.030	500	ST
	31.7192	2.2352	17.496 ± 0.031	300	ST

Table 2. continued.

	Date (UT)	Time since Burst in days	Magnitude (mag)	Exposure time (s)	Telescope
	31.7410	2.257	17.4503 ± 0.028	900	HCT
	31.7414	2.2574	17.509 ± 0.030	300	ST
	31.7598	2.2758	17.508 ± 0.029	300	ST
	31.7740	2.29	17.4403 ± 0.029	900	HCT
	31.7769	2.2929	17.485 ± 0.031	300	ST
	31.7970	2.313	17.520 ± 0.029	300	ST
	31.8046	2.3206	17.4553 ± 0.020	900	HCT
	31.8149	2.3309	17.550 ± 0.028	400	ST
	31.8343	2.3503	17.4853 ± 0.028	900	HCT
	31.8387	2.3547	17.586 ± 0.029	400	ST
	31.8600	2.376	17.595 ± 0.031	400	ST
	31.8806	2.3966	17.617 ± 0.022	400	ST
2003	April				
	1.5967	3.1127	17.866 ± 0.033	300	ST
	1.6277	3.1437	17.749 ± 0.038	200	ST
	1.7153	3.2313	17.826 ± 0.029	400	ST
	1.7207	3.2367	17.831 ± 0.027	400	ST
	1.7356	3.2516	17.7193 ± 0.031	900	HCT
	1.8582	3.3742	17.791 ± 0.037	300	ST
	1.9000	3.416	17.7843 ± 0.034	900	HCT
	2.6386	4.1546	18.3483 ± 0.036	900	HCT
	2.6436	4.1596	18.419 ± 0.041	300	ST
	2.6771	4.1931	18.4003 ± 0.029	900	HCT
	2.6862	4.2022	18.534 ± 0.039	300	ST
	2.7439	4.2599	18.528 ± 0.038	300	ST
	2.7707	4.2867	18.506 ± 0.039	300	ST
	4.6673	6.1833	18.787 ± 0.039	400	ST
	4.6966	6.2126	18.748 ± 0.034	400	ST
	4.7246	6.2406	18.852 ± 0.033	400	ST
	5.6125	7.1285	19.2573 ± 0.067	900	HCT
	5.6511	7.1671	19.2373 ± 0.053	900	HCT
	5.7416	7.2576	19.2963 ± 0.046	900	HCT
	5.7702	7.2862	19.3183 ± 0.044	900	HCT
	5.8037	7.3197	19.3153 ± 0.046	900	HCT
	5.8293	7.3453	19.3683 ± 0.030	900	HCT
	5.8618	7.3778	19.3873 ± 0.045	900	HCT
	6.6438	8.1598	19.6213 ± 0.027	900	HCT
	6.6559	8.1719	19.6443 ± 0.028	900	HCT
	6.7522	8.2682	19.6063 ± 0.030	900	HCT
	6.8384	8.3544	19.6183 ± 0.039	900	HCT
	6.8505	8.3665	19.6553 ± 0.034	900	HCT

Table 2. continued.

	Date (UT)	Time since Burst in days	Magnitude (mag)	Exposure time (s)	Telescope
	7.6122	9.1282	19.761 ± 0.144	400	ST
	8.6260	10.142	19.983 ± 0.069	600	ST
	8.6641	10.1801	19.943 ± 0.076	600	ST
	8.6933	10.2093	19.919 ± 0.064	600	ST
	10.6368	12.1528	20.287 ± 0.087	900	ST
	10.7059	12.2219	20.1933 ± 0.030	600X4	HCT
	11.6782	13.1942	20.432 ± 0.177	600	ST
2003	May				
	1.6271	33.1431	22.214 ± 0.156	3*500+900	ST
		$V-$passband			
2003	March				
	29.6310	0.147	13.8983 ± 0.029	600	HCT
	29.6363	0.1523	13.848 ± 0.020	200	ST
	29.6515	0.1675	13.930 ± 0.023	75	ST
	29.6872	0.2032	14.087 ± 0.021	50	ST
	29.6991	0.2151	14.142 ± 0.017	100	ST
	29.7127	0.2287	14.213 ± 0.018	100	ST
	29.7284	0.2444	14.266 ± 0.033	100	ST
	29.7416	0.2576	14.331 ± 0.018	100	ST
	29.7552	0.2712	14.371 ± 0.032	100	ST
	29.7985	0.3145	14.569 ± 0.032	200	ST
	29.8773	0.3933	14.9323 ± 0.050	600	HCT
	30.6674	1.1834	16.7423 ± 0.047	600	HCT
	30.7486	1.2646	16.7943 ± 0.050	600	HCT
	30.7632	1.2792	16.790 ± 0.013	200	ST
	30.7809	1.2969	16.789 ± 0.013	200	ST
	30.7836	1.2996	16.8153 ± 0.032	600	HCT
	30.7980	1.314	16.773 ± 0.013	200	ST
	30.8202	1.3362	16.825 ± 0.013	200	ST
	30.8256	1.3416	16.8363 ± 0.040	600	HCT
	30.8680	1.384	16.8183 ± 0.046	600	HCT
	30.8998	1.4158	16.8353 ± 0.050	600	HCT
	31.6026	2.1186	17.111 ± 0.013	300	ST
	31.6531	2.1691	17.1033 ± 0.064	600	HCT
	31.6811	2.1971	17.094 ± 0.024	300	ST
	31.7041	2.2201	17.126 ± 0.018	300	ST
	31.7263	2.2423	17.148 ± 0.017	300	ST
	31.7308	2.2468	17.1783 ± 0.055	600	HCT
	31.7459	2.2619	17.150 ± 0.016	300	ST
	31.7589	2.2749	17.1653 ± 0.052	600	HCT

Table 2. continued.

	Date (UT)	Time since Burst in days	Magnitude (mag)	Exposure time (s)	Telescope
	31.7643	2.2803	17.148 ± 0.018	300	ST
	31.7814	2.2974	17.157 ± 0.020	300	ST
	31.7894	2.3054	17.1883 ± 0.040	600	HCT
	31.8015	2.3175	17.179 ± 0.014	300	ST
	31.8211	2.3371	17.212 ± 0.014	400	ST
	31.8216	2.3376	17.2143 ± 0.062	600	HCT
	31.8444	2.3604	17.227 ± 0.016	400	ST
	31.8498	2.3658	17.2443 ± 0.069	600	HCT
	31.8656	2.3816	17.253 ± 0.014	400	ST
	31.8781	2.3941	17.2633 ± 0.055	600	HCT
	31.8862	2.4022	17.253 ± 0.020	400	ST
	31.9177	2.4337	17.2843 ± 0.059	600	HCT
2003	April				
	1.6139	3.1299	17.438 ± 0.017	300	ST
	1.6727	3.1887	17.453 ± 0.017	300	ST
	1.6758	3.1918	17.4463 ± 0.051	450	HCT
	1.7215	3.2375	17.4203 ± 0.051	450	HCT
	1.7326	3.2486	17.453 ± 0.016	400	ST
	1.7381	3.2541	17.464 ± 0.016	400	ST
	1.8841	3.4001	17.427 ± 0.018	300	ST
	1.8847	3.4007	17.4233 ± 0.040	450	HCT
	2.6234	4.1394	18.0493 ± 0.061	450	HCT
	2.6595	4.1755	18.048 ± 0.021	300	ST
	2.6612	4.1772	18.0873 ± 0.065	450	HCT
	2.6903	4.2063	18.0913 ± 0.064	450	HCT
	2.6909	4.2069	18.068 ± 0.020	300	ST
	2.7221	4.2381	18.112 ± 0.024	300	ST
	4.6767	6.1927	18.370 ± 0.024	400	ST
	4.7069	6.2229	18.393 ± 0.025	400	ST
	4.7302	6.2462	18.481 ± 0.023	400	ST
	5.5977	7.1137	18.8733 ± 0.036	450	HCT
	5.6670	7.183	18.8953 ± 0.039	450	HCT
	5.6997	7.2157	18.9383 ± 0.052	450	HCT
	5.7303	7.2463	18.9283 ± 0.055	450	HCT
	5.7573	7.2733	18.9353 ± 0.044	450	HCT
	6.6149	8.1309	19.1813 ± 0.027	600X2	HCT
	6.7218	8.2378	19.2393 ± 0.027	600X3	HCT
	6.8111	8.3271	19.2183 ± 0.046	600X3	HCT
	6.8767	8.3927	19.2253 ± 0.064	600X2	HCT
	7.6073	9.1233	19.294 ± 0.073	300	ST

Table 2. continued.

	Date (UT)	Time since Burst in days	Magnitude (mag)	Exposure time (s)	Telescope
	8.6170	10.133	19.364 ± 0.033	600	ST
	8.6567	10.1727	19.406 ± 0.037	600	ST
	8.6856	10.2016	19.235 ± 0.035	600	ST
	9.5952	11.1112	19.414 ± 0.070	400	ST
	9.6050	11.121	19.5083 ± 0.032	900	HCT
	9.6439	11.1599	19.5233 ± 0.040	900	HCT
	9.6730	11.189	19.5233 ± 0.035	300X2	HCT
	9.7002	11.2162	19.5283 ± 0.044	700	HCT
	9.8625	11.3785	19.5463 ± 0.046	900	HCT
	10.6424	12.1584	19.585 ± 0.067	900	ST
	10.6461	12.1621	19.6303 ± 0.036	900X2	HCT
	10.6656	12.1816	19.6513 ± 0.058	450X3	HCT
	10.7440	12.26	19.6313 ± 0.060	900	HCT
	11.6590	13.175	19.7303 ± 0.043	450X2	HCT
	11.6925	13.2085	19.7763 ± 0.039	450X3	HCT
	11.6975	13.2135	19.951 ± 0.174	600	ST
	22.6520	24.168	20.5103 ± 0.048	600X3	HCT
	23.6646	25.1806	20.6343 ± 0.050	300X2+600	HCT
2003	May				
	1.6383	33.1543	20.836 ± 0.123	900	ST
			$R-$passband		
2003	March				
	29.6133	0.1293	13.3803 ± 0.031	120	HCT
	29.6171	0.1331	13.3743 ± 0.041	300	HCT
	29.6227	0.1387	13.431 ± 0.032	100	ST
	29.6232	0.1392	13.4123 ± 0.060	450	HCT
	29.6264	0.1424	13.422 ± 0.025	200	ST
	29.6397	0.1557	13.506 ± 0.024	200	ST
	29.6483	0.1643	13.577 ± 0.024	50	ST
	29.6530	0.169	13.619 ± 0.034	50	ST
	29.6572	0.1732	13.636 ± 0.040	100	ST
	29.6701	0.1861	13.7243 ± 0.034	600	HCT
	29.6784	0.1944	13.7233 ± 0.044	600	HCT
	29.6839	0.1999	13.724 ± 0.025	50	ST
	29.6863	0.2023	13.7893 ± 0.031	600	HCT
	29.6967	0.2127	13.829 ± 0.026	100	ST
	29.7103	0.2263	13.854 ± 0.026	100	ST

Table 2. continued.

Date (UT)	Time since Burst in days	Magnitude (mag)	Exposure time (s)	Telescope
29.7262	0.2422	13.916 ± 0.026	100	ST
29.7396	0.2556	13.982 ± 0.027	100	ST
29.7526	0.2686	14.030 ± 0.027	100	ST
29.7650	0.281	14.098 ± 0.052	200	ST
29.7937	0.3097	14.210 ± 0.032	100	ST
29.8675	0.3835	14.4893 ± 0.050	600	HCT
29.8857	0.4017	14.5483 ± 0.046	600	HCT
29.9079	0.4239	14.6333 ± 0.032	450	HCT
29.9140	0.43	14.6533 ± 0.033	450	HCT
29.9201	0.4361	14.6613 ± 0.040	450	HCT
29.9275	0.4435	14.6753 ± 0.070	450	HCT
30.5833	1.0993	16.249 ± 0.070	100	ST
30.5875	1.1035	16.295 ± 0.056	200	ST
30.6518	1.1678	16.2963 ± 0.070	180	HCT
30.6586	1.1746	16.3343 ± 0.042	600	HCT
30.6747	1.1907	16.3533 ± 0.039	450	HCT
30.6879	1.2039	16.3733 ± 0.028	450	HCT
30.7268	1.2428	16.3723 ± 0.049	450	HCT
30.7637	1.2797	16.4133 ± 0.040	450	HCT
30.7665	1.2825	16.420 ± 0.021	200	ST
30.7841	1.3001	16.438 ± 0.018	200	ST
30.7971	1.3131	16.4223 ± 0.050	450	HCT
30.8012	1.3172	16.439 ± 0.018	200	ST
30.8176	1.3336	16.4453 ± 0.041	450	HCT
30.8238	1.3398	16.460 ± 0.017	200	ST
30.8457	1.3617	16.4593 ± 0.039	450	HCT
30.8603	1.3763	16.4683 ± 0.034	450	HCT
30.8759	1.3919	16.4623 ± 0.032	450	HCT
30.8914	1.4074	16.4613 ± 0.039	450	HCT
30.9076	1.4236	16.4353 ± 0.057	450	HCT
30.9142	1.4302	16.4703 ± 0.034	450	HCT
30.9212	1.4372	16.4303 ± 0.031	450	HCT
30.9276	1.4436	16.4013 ± 0.063	450	HCT
31.6449	2.1609	16.7163 ± 0.040	450	HCT
31.6610	2.177	16.7163 ± 0.031	450	HCT
31.6653	2.1813	16.711 ± 0.032	100	ST
31.6804	2.1964	16.7103 ± 0.041	450	HCT
31.6898	2.2058	16.744 ± 0.033	200	ST

Table 2. continued.

	Date (UT)	Time since Burst in days	Magnitude (mag)	Exposure time (s)	Telescope
	31.7083	2.2243	16.771 ± 0.031	200	ST
	31.7148	2.2308	16.783 ± 0.027	300	ST
	31.7231	2.2391	16.7823 ± 0.026	450	HCT
	31.7303	2.2463	16.772 ± 0.027	200	ST
	31.7500	2.266	16.779 ± 0.026	200	ST
	31.7507	2.2667	16.7953 ± 0.040	450	HCT
	31.7655	2.2815	16.7933 ± 0.035	300	HCT
	31.7682	2.2842	16.788 ± 0.029	200	ST
	31.7826	2.2986	16.7953 ± 0.043	300	HCT
	31.7853	2.3013	16.798 ± 0.029	200	ST
	31.7943	2.3103	16.8203 ± 0.025	300	HCT
	31.8054	2.3214	16.820 ± 0.025	200	ST
	31.8139	2.3299	16.8083 ± 0.034	300	HCT
	31.8264	2.3424	16.8443 ± 0.043	300	HCT
	31.8280	2.344	16.844 ± 0.024	300	ST
	31.8431	2.3591	16.8503 ± 0.040	300	HCT
	31.8495	2.3655	16.867 ± 0.024	300	ST
	31.8545	2.3705	16.8583 ± 0.048	300	HCT
	31.8705	2.3865	16.874 ± 0.024	300	ST
	31.8713	2.3873	16.8573 ± 0.044	300	HCT
	31.8832	2.3992	16.8683 ± 0.045	300	HCT
	31.8912	2.4072	16.900 ± 0.023	300	ST
	31.8999	2.4159	16.8723 ± 0.059	300	HCT
	31.9111	2.4271	16.9013 ± 0.037	300	HCT
	31.9223	2.4383	16.9163 ± 0.028	300	HCT
2003	April				
	1.6008	3.1168	17.071 ± 0.027	200	ST
	1.6237	3.1397	17.045 ± 0.025	300	ST
	1.6569	3.1729	17.059 ± 0.025	200	ST
	1.6694	3.1854	17.0553 ± 0.046	300	HCT
	1.6766	3.1926	17.075 ± 0.026	200	ST
	1.6821	3.1981	17.0453 ± 0.045	300	HCT
	1.6950	3.211	17.079 ± 0.026	200	ST
	1.7274	3.2434	17.0473 ± 0.037	300	HCT
	1.7445	3.2605	17.0583 ± 0.032	300	HCT
	1.7487	3.2647	17.075 ± 0.029	300	ST
	1.7531	3.2691	17.071 ± 0.026	300	ST
	1.8628	3.3788	17.058 ± 0.023	300	ST
	1.8891	3.4051	17.039 ± 0.024	300	ST
	1.8906	3.4066	17.0273 ± 0.035	300	HCT

Table 2. continued.

Date (UT)	Time since Burst in days	Magnitude (mag)	Exposure time (s)	Telescope
1.9103	3.4263	17.101 ± 0.028	300	ST
2.6158	4.1318	17.6723 ± 0.046	300	HCT
2.6391	4.1551	17.694 ± 0.028	300	ST
2.6425	4.1585	17.6933 ± 0.029	300	HCT
2.6531	4.1691	17.7113 ± 0.029	300	HCT
2.6553	4.1713	17.707 ± 0.025	300	ST
2.6697	4.1857	17.680 ± 0.027	300	ST
2.6843	4.2003	17.7193 ± 0.033	300	HCT
2.6953	4.2113	17.689 ± 0.028	300	ST
2.6962	4.2122	17.7023 ± 0.033	300	HCT
2.7124	4.2284	17.706 ± 0.034	300	ST
2.7265	4.2425	17.709 ± 0.030	300	ST
2.7484	4.2644	17.721 ± 0.030	300	ST
2.7615	4.2775	17.737 ± 0.030	300	ST
2.7752	4.2912	17.718 ± 0.032	300	ST
4.6831	6.1991	18.030 ± 0.031	400	ST
4.7125	6.2285	18.085 ± 0.035	400	ST
4.7357	6.2517	18.130 ± 0.031	400	ST
5.5919	7.1079	18.4583 ± 0.049	300	HCT
5.6044	7.1204	18.5093 ± 0.028	300	HCT
5.6209	7.1369	18.5033 ± 0.025	300	HCT
5.6340	7.15	18.4963 ± 0.032	300	HCT
5.6603	7.1763	18.4803 ± 0.036	300	HCT
5.6858	7.2018	18.5763 ± 0.029	300	HCT
5.7054	7.2214	18.5873 ± 0.024	300	HCT
5.7231	7.2391	18.5243 ± 0.029	300	HCT
5.7507	7.2667	18.5683 ± 0.027	300	HCT
5.7790	7.295	18.5873 ± 0.027	300	HCT
5.7949	7.3109	18.5803 ± 0.036	300	HCT
5.8130	7.329	18.6003 ± 0.027	300	HCT
5.8454	7.3614	18.5893 ± 0.035	300	HCT
5.8704	7.3864	18.6283 ± 0.037	300	HCT
5.9002	7.4162	18.6643 ± 0.049	300	HCT
6.5919	8.1079	18.8233 ± 0.039	300	HCT
6.5995	8.1155	18.8373 ± 0.029	300	HCT
6.6234	8.1394	18.8053 ± 0.036	300	HCT
6.6849	8.2009	18.8453 ± 0.025	600	HCT
6.6932	8.2092	18.8503 ± 0.030	600	HCT

Table 2. continued.

	Date (UT)	Time since Burst in days	Magnitude (mag)	Exposure time (s)	Telescope
	6.7327	8.2487	18.8503 ± 0.032	600	HCT
	6.7413	8.2573	18.8443 ± 0.022	600	HCT
	6.7792	8.2952	18.8363 ± 0.029	600	HCT
	6.7878	8.3038	18.8433 ± 0.034	600	HCT
	6.8205	8.3365	18.8523 ± 0.029	600	HCT
	6.8286	8.3446	18.8473 ± 0.047	600	HCT
	6.8851	8.4011	18.8823 ± 0.043	600	HCT
	6.8935	8.4095	18.8773 ± 0.038	600	HCT
	6.9016	8.4176	18.8183 ± 0.031	600	HCT
	7.5936	9.1096	18.897 ± 0.052	300	ST
	7.5980	9.114	18.945 ± 0.067	300	ST
	8.6070	10.123	19.017 ± 0.046	400	ST
	8.6483	10.1643	19.049 ± 0.041	600	ST
	8.6778	10.1938	19.064 ± 0.032	600	ST
	9.5890	11.105	19.078 ± 0.057	400	ST
	9.5905	11.1065	19.1263 ± 0.033	900	HCT
	9.6321	11.1481	19.0963 ± 0.037	900	HCT
	9.6875	11.2035	19.1403 ± 0.037	300X2	HCT
	9.7242	11.2402	19.1743 ± 0.039	300X3	HCT
	9.8502	11.3662	19.1663 ± 0.050	900	HCT
	10.6068	12.1228	19.3113 ± 0.030	900	HCT
	10.6157	12.1317	19.440 ± 0.095	400	ST
	10.6437	12.1597	19.2923 ± 0.052	900	HCT
	10.6483	12.1643	19.294 ± 0.057	900	ST
	10.6825	12.1985	19.2553 ± 0.050	300X3	HCT
	10.7272	12.2432	19.3483 ± 0.039	300+450	HCT
	10.7390	12.255	19.3503 ± 0.041	300	HCT
	10.7574	12.2734	19.3283 ± 0.049	900	HCT
	10.8689	12.3849	19.3463 ± 0.060	900	HCT
	11.6743	13.1903	19.4273 ± 0.038	300X3	HCT
	11.7064	13.2224	19.527 ± 0.154	600	ST
	11.7082	13.2242	19.2813 ± 0.053	300X2	HCT
	22.6028	24.1188	20.1233 ± 0.043	600	HCT
	22.6279	24.1439	20.0573 ± 0.040	600X2	HCT
	22.8033	24.3193	20.0633 ± 0.025	600X3	HCT
	23.6311	25.1471	20.0983 ± 0.032	300X5	HCT
2003	May				
	1.6069	33.1229	±20.692 ± 0.090	2*300	ST

Table 2. continued.

	Date (UT)	Time since Burst in days	Magnitude (mag)	Exposure time (s)	Telescope
		$I-$passband			
2003	March				
	29.6306	0.1466	13.037 ± 0.026	200	ST
	29.6499	0.1659	13.185 ± 0.029	50	ST
	29.6855	0.2015	13.328 ± 0.029	50	ST
	29.6948	0.2108	13.487 ± 0.031	50	ST
	29.7083	0.2243	13.437 ± 0.030	100	ST
	29.7241	0.2401	13.501 ± 0.032	100	ST
	29.7374	0.2534	13.559 ± 0.032	100	ST
	29.7504	0.2664	13.618 ± 0.032	100	ST
	29.7616	0.2776	13.685 ± 0.032	200	ST
	29.7959	0.3119	13.837 ± 0.049	100	ST
	30.7698	1.2858	15.972 ± 0.023	200	ST
	30.7872	1.3032	15.985 ± 0.021	200	ST
	30.8046	1.3206	15.978 ± 0.021	200	ST
	30.8272	1.3432	16.058 ± 0.021	200	ST
	31.6683	2.1843	16.240 ± 0.034	100	ST
	31.6933	2.2093	16.290 ± 0.033	200	ST
	31.7110	2.227	16.305 ± 0.034	200	ST
	31.7338	2.2498	16.342 ± 0.031	200	ST
	31.7535	2.2695	16.329 ± 0.031	200	ST
	31.7715	2.2875	16.326 ± 0.033	200	ST
	31.7887	2.3047	16.341 ± 0.030	200	ST
	31.8088	2.3248	16.351 ± 0.030	200	ST
	31.8326	2.3486	16.387 ± 0.029	300	ST
	31.8539	2.3699	16.411 ± 0.028	300	ST
	31.8750	2.391	16.404 ± 0.028	300	ST
	31.8960	2.412	16.460 ± 0.028	300	ST
2003	April				
	1.6086	3.1246	16.591 ± 0.032	200	ST
	1.6890	3.205	16.586 ± 0.033	200	ST
	1.8294	3.3454	16.639 ± 0.029	300	ST
	1.8338	3.3498	16.631 ± 0.029	300	ST
	2.6738	4.1898	17.211 ± 0.031	300	ST
	2.7077	4.2237	17.224 ± 0.032	300	ST
	2.7572	4.2732	17.254 ± 0.035	300	ST
	4.6886	6.2046	17.586 ± 0.046	400	ST
	4.7180	6.234	17.663 ± 0.042	400	ST
	7.6029	9.1189	18.595 ± 0.098	300	ST
	8.5965	10.1125	18.674 ± 0.077	400	ST
	8.6405	10.1565	18.764 ± 0.052	600	ST
	8.6712	10.1872	18.614 ± 0.064	400	ST